In silico studies and fluorescence binding assays of potential anti-prion compounds reveal an important binding site for prion inhibition from PrPC to PrPSc

4 **AUTHORS**, INCLUDING:

Pagadala Nataraj Sekhar
University of Alberta
21 PUBLICATIONS **95** CITATIONS

SEE PROFILE

Rolando Pérez-Pineiro
M-I Swaco a Schlumberger company
58 PUBLICATIONS **969** CITATIONS

SEE PROFILE

Jack Adam Tuszynski
University of Alberta
307 PUBLICATIONS **3,073** CITATIONS

SEE PROFILE

Original article

In silico studies and fluorescence binding assays of potential anti-prion compounds reveal an important binding site for prion inhibition from PrP^C to PrP^{Sc}

Nataraj S. Pagadala [a], Rolando Perez-Pineiro [b], David S. Wishart [b], Jack A. Tuszynski [c, *]

[a] *Department of Medical Microbiology and Immunology, 6-020 Katz Group Centre, University of Alberta, Edmonton, Alberta T6G 2E1, Canada*
[b] *Departments of Biological Sciences, and Computing Science, University of Alberta, Edmonton, Alberta T6G 2E8, Canada*
[c] *Department of Physics, University of Alberta, Edmonton, Alberta T6G 2J1, Canada*

A B S T R A C T

To understand the pharmacophore properties of 2-aminothiazoles and design novel inhibitors against the prion protein, a highly predictive 3D quantitative structure–activity relationship (QSAR) has been developed by performing comparative molecular field analysis (CoMFA) and comparative similarity analysis (CoMSIA). Both CoMFA and CoMSIA maps reveal the presence of the oxymethyl groups in meta and para positions on the phenyl ring of compound **17** (N-[4-(3,4-dimethoxyphenyl)-1,3-thiazol-2-yl] quinolin-2-amine), is necessary for activity while electro-negative nitrogen of quinoline is highly favorable to enhance activity. The blind docking results for these compounds show that the compound with quinoline binds with higher affinity than isoquinoline and naphthalene groups. Out of 150 novel compounds retrieved using finger print analysis by pharmacophoric model predicted based on five test sets of compounds, five compounds with diverse scaffolds were selected for biological evaluation as possible PrP inhibitors. Molecular docking combined with fluorescence quenching studies show that these compounds bind to pocket-D of SHaPrP near Trp145. The new antiprion compounds **3** and **6**, which bind with the interaction energies of -12.1 and -13.2 kcal/mol, respectively, show fluorescence quenching with binding constant (K_d) values of 15.5 and 44.14 μM, respectively. Further fluorescence binding assays with compound **5**, which is similar to 2-aminothiazole as a positive control, also show that the molecule binds to the pocket-D with the binding constant (K_d) value of 84.7 μM. Finally, both molecular docking and a fluorescence binding assay of noscapine as a negative control reveals the same binding site on the surface of pocket-A near a rigid loop between β2 and α2 interacting with Arg164. This high level of correlation between molecular docking and fluorescence quenching studies confirm that these five compounds are likely to act as inhibitors for prion propagation while noscapine might act as a prion accelerator from PrP^C to PrP^{Sc}.

© 2014 Published by Elsevier Masson SAS.

1. Introduction

Transmissible spongiform encephalopathies (TSEs) or prion diseases are characterized by accumulation of a protease resistant form of the prion protein in the brain [1,2]. Studies have shown that brain disease arises when the normal cellular prion protein PrP^C, which is α-helix rich, is converted into an abnormally folded, disease-related isoform PrP^{Sc}, which is β-sheet rich [3]. TSEs are invariably fatal and currently no effective therapies or vaccines exist. Consequently, numerous studies have been directed toward the development of therapeutics for preventing the conversion of PrP^c to PrP^{sc} involved in neural degeneration despite the lack of a detailed understanding of the cellular mechanism of prion propagation. The potential strategy for therapeutic intervention of prion disease is to maintain structural stability towards conformational change by binding to PrP^C [4]. To date, various compounds such as polyanionic agents, Congo red, amphotericin B, porphyrins, and phenothiazine derivatives, such as quinacrine have been shown to reduce PrP^{sc} accumulation in a cell culture model of prion diseases [5]. In addition, other molecules that are of polyanionic chemotype (suramin, pentosan polysulfate) or

* Corresponding author. Department of Physics, University of Alberta, Edmonton, Alberta T6G 2V4, Canada.
E-mail addresses: jackt@ualberta.ca, jack.tuszynski@gmail.com (J.A. Tuszynski).

polycationic chemotype (dendritic polyamines, cationic polysaccharides) have been reported to show antiprion activity in cells but are not used therapeutically [6]. Studies on quinacrine along with lysomotropic agents and cysteine protease inhibitors demonstrated it to be a potent inhibitor of prion disease in cultured neuroblastoma cells [7]. Due to high toxicity, quinacrine was considered an unsuitable drug for prion disease although it inhibits accumulation of PrP^{Sc} in neuroblastoma cells [8]. This molecule along with analogs of acridine, phenothiazine and other tricyclic compounds, binds to PrP^{C} via specific amino acid residues [9]. Some of the natural products and known drugs that include analogs of bicyclic- and tricyclic-nitrogen containing aromatic systems such as quinoline, acridine and phenothiazine display IC50s in the nanomolar range in high-throughput screening assays [3]. The activity of the compounds, phenothiazines, acridines and quinolines in prion studies is mainly through aliphatic side chains [10,11]. The compound pyrazolone has been shown to be up to 130 fold more effective compared to quinacrine in inhibiting the accumulation of PrP^{sc} [12]. Recently, the compound "GN8" using NMR chemical shifts was also demonstrated to interact with the C-terminal domain of PrP^{C} [13]. However, none of these molecules has yet been proved to be more effective against a variety of prion strains in an animal model of this disease. One possible explanation for this poor record is that most small molecules investigated to date were originally designed for other purposes (for example, malaria, and hyperlipidemia) and not optimized either for anti-prion effects or for the ability to cross the blood−brain barrier (BBB). The compounds, 2-aminothiazoles, which represent a promising new class of drugs for prion diseases show potent inhibitory activities against PrP^{C}. The compound **17** (see Table 3) is a typical example among them (EC$_{50}$ values for prion proteins are in the 0.1 μM range), which provided a solid foundation for the design of new selective inhibitors against prion proteins [14]. In order to discover novel anti-prion compounds against SHaPrP using a set of 2-amino thiazoles, 3D QSAR models were built using a comparative molecular field analysis (CoMFA) and comparative molecular similarity analysis (CoMSIA). These 2-aminothiazole compounds were further docked against the four represented models of SHaPrP. The correlation of the binding energies with experimentally determined EC$_{50}$ values was analyzed to predict the accurate binding site of SHaPrP. The pharmacophoric model that was generated using GALAHAD was used as a scaffold for similarity search against the MOE database. The compounds with ≥85% level of similarity were retrieved and used for further docking studies. These virtually screened compounds that displayed variation in the location and nature of side chains were analyzed for binding with SHaPrP. In total, five compounds with different scaffolds that bind with high, medium and low affinity were selected for further fluorescence titration experiments. In order to validate our computational and experimental results, the known compound noscapine, which is effective in crossing the blood−brain barrier with a potent central nervous system activity similar to the ones found for agents such as morphine and [Met]encephalin, was docked and tested experimentally using a fluorescence quenching binding assay against SHaPrP. To the best of our knowledge, no previous studies have been conducted to find a new insight into the relationship between structural information and the inhibitory potency and selectivity of 2-aminothiazoles. The objective of this study was: (i) to demonstrate the binding modes of 2-aminothiazoles, with SHaPrP, (ii) to explain the SAR data for SHaPrP inhibitors based on structural features associated with the chemical modifications of the compounds and (iii) to predict the binding affinities and K_{d} values of these new compounds using computational and fluorescence titration experiments.

2. Results and discussion

2.1. CoMFA

The structural diversity and changes in biological activity were first studied using 2-amino thiazoles. Since the inhibitors against the prion protein are very limited regarding known biological activity, the study was restricted to the very limited number of compounds for prion disease. The pharmacophore alignment generated from GALAHAD was used to develop the CoMFA model for 37 prion inhibitors (see Fig. 1a). The optimum model is associated with six pharmacophore features consisting of two hydrophobic centers (HY1 and HY2), an H-bond acceptor (AA1) and an H-bond donor (DA1) (see Fig. 1b). The best CoMFA model was selected based on their statistical parameters. Pharmacophore-based alignment produces the CoMFA model with a q^2 of 0.9, r^2 of 0.97 and 0.128 as standard error of estimate (see Table 1). This CoMFA based model is used to predict EC$_{50}$ values for all the compounds as shown in Table 2. The graph of predicted versus measured pEC_{50} asset value is presented in Fig. 2a. The CoMFA model was further evaluated for its robustness and statistical confidence by bootstrap analysis for 10 runs. In a bootstrap analysis, many new data sets are derived from the original set by randomly choosing samples. The value obtained for r^{2boot} of 0.9 with a standard deviation of 0.009 suggests a good consistency for the dataset. Moreover, the stability of the model was predicted with cross-validation analysis using the leave-one-out method. The value of r^2 CV 0.9 shows that the model predicted using CoMFA is highly reliable for further studies. The contour maps of CoMFA generated from the 3D QSAR models built using pharmacophore based alignment highlight the interaction sites responsible for differences in the biological activity. Green indicates the contour regions where the bulky substituent would increase the inhibitory activity, while the yellow outline indicates the regions where steric bulk would be unfavorable to the inhibitory activity of prion proteins. CoMFA contour maps of the steric and electrostatic properties of compound **17** give the highest affinity of the series (0.11 μM) as shown in Fig. 3a. The large green contour found around the quinoline group of **17** indicates that a
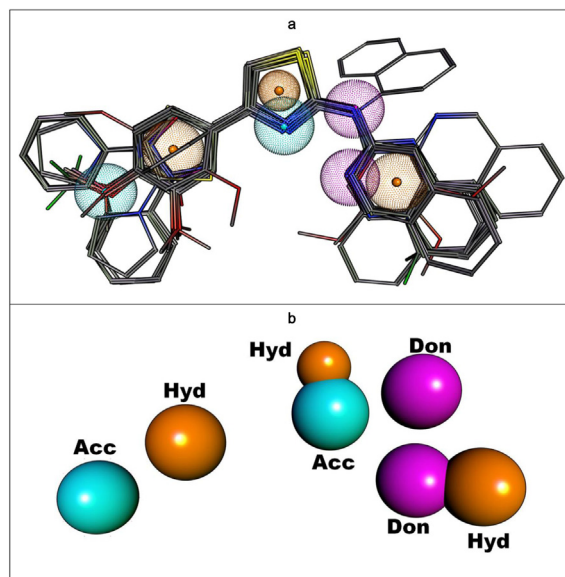

Fig. 1. a: The alignment of the molecules in the present study. b: pharmacophore hypothesis of the aligned molecules using GALAHAD; magenta, hydrogen bond donor atom (D); Cyan, acceptor atom (A); and Orange, hydrophobic center (H). (For interpretation of the references to color in this figure legend, the reader is referred to the web version of this article.)

Table 1
Statistical results of CoMFA, COMSIA analysis for 2-amino thiazoles as antiprion compounds.

PLS statistics	COMFA	CoMSIA
Components	6	6
q^2 Loo	0.964	0.91
Conventional r^2	0.967	0.92
Standard error of estimate	0.124	0.17
F values	148.554	432.764
Bootstrapping		
r^2	0.98	0.93
Standard error of estimate boot strapping	0.08	0.156
Progress scrambling		
Q^2	0.78	0.71
cSDEP	0.31	0.33
$dq^{2'}/dr^2_{yy'}$	1.15	1.26
Predictive r^2	0.71	0.74
Fraction		
Steric	0.95	0.51
Electrostatic	0.89	0.34
Hydrophobic	–	0.38
Hydrogen bond donor	–	0.17
Hydrogen bond acceptor	–	0.27
Steric and electrostatic		0.439
Donar and acceptor		0.389

bulky group at this position provides support for the high biological activity. The equal occupancy of sterically favorable green contour for isoquinoline (compound **18** (see Fig. 3b) and 1-substitute naphthalene (compound **19**) (see Fig. 3c) derivatives allow these compounds to show higher biological activities with 0.43 and 0.39 μM, respectively, next to quinoline with 0.11 μM. The green contour is far from the 2-substituted naphthalene ring (compound **20**) and it shows a poor inhibition activity given by >32 μM (see Fig. 3d). This is perhaps why the 1-substituted bicyclic compounds, quinoline, isoquinoline and napthalene (e.g., compounds **17**–**19**, **30**–**37**) that occupy the green contour are more potent than 2-substituted napthalene. The phenyl and pyridinyl-substituted compounds **5**–**16** are located slightly away from the green contour showing moderate potency. The substituent of the quinoline with triflouro methoxy benzene in the R^2 position of compound **31** does not affect the orientation of quinoline away from the green contour but is less potent than the quinoline compound due to the absence of an oxymethyl group in the para position with >32 μM (see Fig. 3e). Conversely, the quinoline ring of the most potent compound **17** shows least proximity to the yellow contour. Substitution of the quinoline with isoquinoline reduces the inhibitory activity of the compound **18** (see Fig. 3b). The presence of yellow contours near the oxymethyl group of 1-substituted naphthalene indicates it is unfavorable for the biological activity. Moreover, the unfavorable yellow contour was observed near the oxymethyl and naphthalene group of the least potent compound (compound **20**) (EC$_{50}$ ≥ 32 μM). This indicates that a 2-substituted naphthalene would significantly reduce the binding affinity with >32 μM. The oxymethyl groups in compounds **31** and **36** is substituted by trifluoro and a methyl group that leads to a decrease in activity with >32 μM (see Fig. 3e and f). Therefore, the presence of a yellow contour around trifluoro shows that the size of substitution at this position is crucial for inhibitory activity. The substituents at R, R^1 and R^2, are seen to have varying distances from the yellow contour groups but their close proximity explains their low potency. There is a significant loss of activity in the 2-naphthyl ring-substituted compound **20** (EC$_{50}$ ≥ 32 μM), as compared to the 1-naphthyl ring-substituted compound 19 (EC$_{50}$ = 0.3 μM). The 2-naphthyl group was close to the unfavorable yellow contour showing a bulky group on this site would be unfavorable for higher activity. The CoMFA electrostatic contour map marked by red and blue

contours, including red regions show areas where more negatively charged groups are favorable to inhibitory activity and blue colored regions represent areas where increased positively charged groups are favorable to activity. The red contour map near an oxymethyl group indicates that electronegative group is favored at the meta position of the phenyl ring. This has been well supported since compounds having oxymethyl group (electronegative) in the meta position showed higher activity (compound **30**) than other substitutions (compounds **31**–**37**). The phenyl and oxymethyl portion of the quinoline and isoquinoline moiety of compounds (compounds **17**, **18**) are occupied by large blue contours due to the presence of the electron-withdrawing pyridine ring and electron-donating oxymethyl group of the quinoline and isoquinoline moieties. The large blue contour shows that an electron-deficient nature is important for high binding affinity. The electronegative carbonyl oxygen atom of the oxymethyl group forms a favorable contact with the positively charged nitrogen atom of Asn197 surrounded by a blue contour. The electrostatic interactions with these backbone atoms are essential for differentiation in potencies of compounds with bicyclic rings such as with a substituted naphthyl (compounds **19**, **20**) and quinolinyl rings (compounds **18**, **31**, **36**). The high-potency compounds (**17**, **19**) (EC$_{50}$ = 0.11 and 0.39 μM, respectively) having 3, 4-dimethoxyphenyl ring substitutions show a favorable electropositive methyl group of oxymethyl function in the vicinity of a blue contour. The oxymethyl groups are responsible for the differences between the compounds **17**, **19** with **18**, **20**, **31** and **36**. The two medium-size blue contours were found to be situated on each side of the plane of the thiazole ring. The naphthalene moiety of the compound **20** is mapped away from these blue contours, which accounts for the significant loss of activity. This suggests that the electropositive nature of the ring is essential for activity. Although the red contour was found near the oxymethyl and trifluoro groups in compounds **20** and **31**, there is a steric clash of the thiazole rings of these two compounds with the side chain −SCH3 of Met206. Thus, the 2-substituted naphthalene and quinoline containing compounds such as **20** and **31** show least potency. The methyl group of the compound **36** is too far away from these red contours showing least potency with >32 μM. The increased activity of compound **17** is due to the presence of the electronegative oxygen atoms with the partial atomic charge of −0.345 compared to **31** with the electropositive nature of a carbon atom of the trifluoro with the partial atomic charge of +0.529. The red contours with the high electron density of the compound **17** are in close proximity to the electronegative group of Met206-SCH3 justifying the presence of red and yellow contours.

2.2. CoMSIA

The protocol generated for CoMFA models was used to study CoMSIA using the same information generated from pharmacophore alignment. The best CoMSIA model with a q^2 value of 0.9 was obtained using the hydrophobic-steric, electrostatic fields, hydrogen bond donor and acceptor fields (see Table 1). This means that all the fields not only contribute to a high value of q^2 but also increase the correlation. This CoMSIA-based model is used to predict EC$_{50}$ values for all the compounds as shown in Table 2. The graph of predicted versus measured pEC$_{50}$ asset values is presented in Fig. 2b. The predictive r^2 of 0.8 and statistical error in the fraction of 101.3 indicates that the model is very reliable. The observed versus predicted values for training and test sets are presented in Table 2. The CoMSIA model generated five physico-chemical properties that reflect the positive contributions to the biological activity for the most potent and less potent compounds, which are shown in Fig. 4. A green and two yellow contours of CoMSIA steric map can be well compared with steric contour maps of CoMFA.

Table 2
Predicted EC$_{50}$ values for the 2-amino thiazole analogs using CoMFA, and CoMSIA analysis.

Comp	Exp data	CoMFA	CoMSIA
		Predicted	Predicted
17	6.9586	6.774	6.791
40	6.6383	6.548	6.638
41	6.6021	6.579	6.587
32	6.5086	6.504	6.340
30	6.4685	6.419	6.577
19	6.4089	6.449	6.253
18	6.3665	6.452	6.224
42	6.2218	6.193	6.135
14	6.1024	5.940	5.939
35	6.0969	6.180	6.376
44	6.0862	6.206	6.163
24	6.0655	5.943	5.842
27	6.0269	5.994	6.085
13	6.0000	5.903	5.874
16	6.0000	6.102	5.962
7	5.9136	5.576	5.446
26	5.9101	5.902	5.772
43	5.8962	5.962	5.749
11	5.8069	5.890	5.918
23	5.8041	5.951	5.979
34	5.6968	5.856	5.719
12	5.5969	5.420	5.601
8	5.5528	5.709	5.633
22	5.5376	5.422	5.491
10	5.5376	5.704	5.846
4	5.5214	5.505	5.547
21	5.5186	5.616	5.652
33	5.5114	5.584	5.830
45	5.3546	5.359	5.128
9	5.1952	5.166	5.244
15	5.1373	5.112	5.405
47	5.0872	5.089	5.175
6	5.0862	5.232	5.388
36	4.4949	4.480	4.494
20	4.4949	4.518	4.503
5	4.4949	4.562	4.479
31	4.4949	4.393	4.409

Likewise, the electrostatic contour map of CoMSIA shows red contours around the compounds **17**–**20**, **31** and **36** (see Fig. 4a–e). The red contour near the biphenyl groups except 2-substituted naphthalene indicates that these groups are favorable for inhibitory activity. Experimental data also show that these biphenyl groups are essential for the inhibition of prion aggregation. The quinoline substituent of compound **17** (EC$_{50}$ = 0.11 μM) showed an increased potency over compounds **18**–**20**, **31** and **36** due to the presence of quinoline and oxymethyl groups. Orientation of quinoline plays an important role in increasing the inhibitory potency compared to other compounds. The substitution of quinoline with isoquinoline and napthalene showed decreased binding affinity, which indicates that a nitrogen atom in the second position is essential for binding affinity (see Fig. 4a). In the case of compound **20** (EC$_{50}$ ≥ 32 μM), lack of nitrogen and substitution of naphthalene at the second position resulted in loss of potency (see Fig. 4c). This shows that the nitrogen atom in the quinoline group is important for high inhibitory potency. The presence of the quinoline group had a slightly better effect on the inhibitory potency than a 1-substitute naphthalene group of 2-amino thiazoles (see Fig. 5b and d). The hydrophobic group which plays an important role in biological activity shown in yellow contours indicates favorable regions of activity whereas favored hydrophilic groups are shown in white contours indicating disfavored regions for inhibitory activity. Fig. 4 depicts the hydrophobic contour maps for these compounds **17**–**20**, **31** and **36** (see Fig. 5a–e). The yellow contour is

found close to the quinolone (see Fig. 4a), isoquinolone (see Fig. 5b), and 1-substituted naphthalene (see Fig. 5c), which could enable hydrophobic interactions with side chains of Met134, Met154, Ile205 and Val209 (see Fig. 4a–c). A small white contour near the oxymethyl group indicates that the substitution of the hydrophobic group may affect inhibitory potency (see Fig. 4f). In CoMSIA, the hydrogen-bond-donor field colored by cyan describes areas where hydrogen-bond-acceptor groups should be located on the receptor. The nitrogen atom between the thiazole and quinoline group is favorable for hydrogen bond donor, which is nearer to Met206 containing an electro-negative group -SCH3. A small magenta color contour near the nitrogen atom of the quinoline indicates that the nitrogen atom acts as an H-bond acceptor. Large red-colored contours occur near the hydrogen atoms of quinoline and thiazole groups and indicate that these positions are unfavorable for the H-bond acceptor group.

2.3. Docking studies of 2-aminothiazoles

The half maximal effective concentration values (EC$_{50}$) available for a series of 2-amino thiazoles (see Table 3) were compared with docking scores for the four represented models to design new and efficient anti-prion compounds [15]. By comparison of docking scores and the EC$_{50}$ values measured experimentally it is possible: (1) to test the binding affinity of the inhibitors and (2) to derive an equation for determining the theoretical EC$_{50}$ values (pEC$_{50}$) for new molecules. The relative EC$_{50}$ values were calculated using the equation, $\Delta \log EC_{50} = \log EC_{50}$ (inhibitor) $- \log EC_{50}$ (compound **17**). The docking scores of these molecules calculated using the Tripos force field are shown in Table 3. The compound **17** showed a
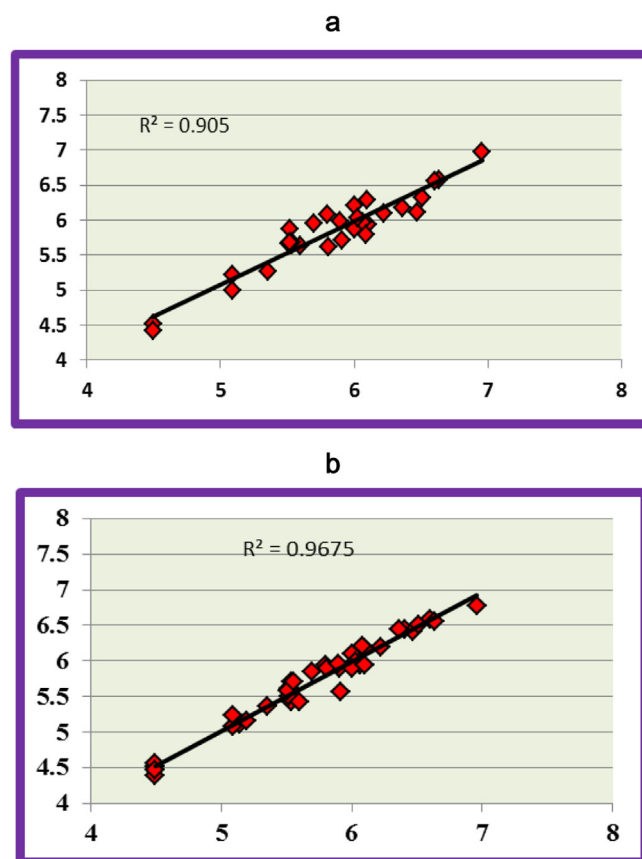
Fig. 2. Scatter plot diagram of predicted versus actual activity of 2-aminothiazole compounds by a: CoMFA, and b: CoMSIA analyses.
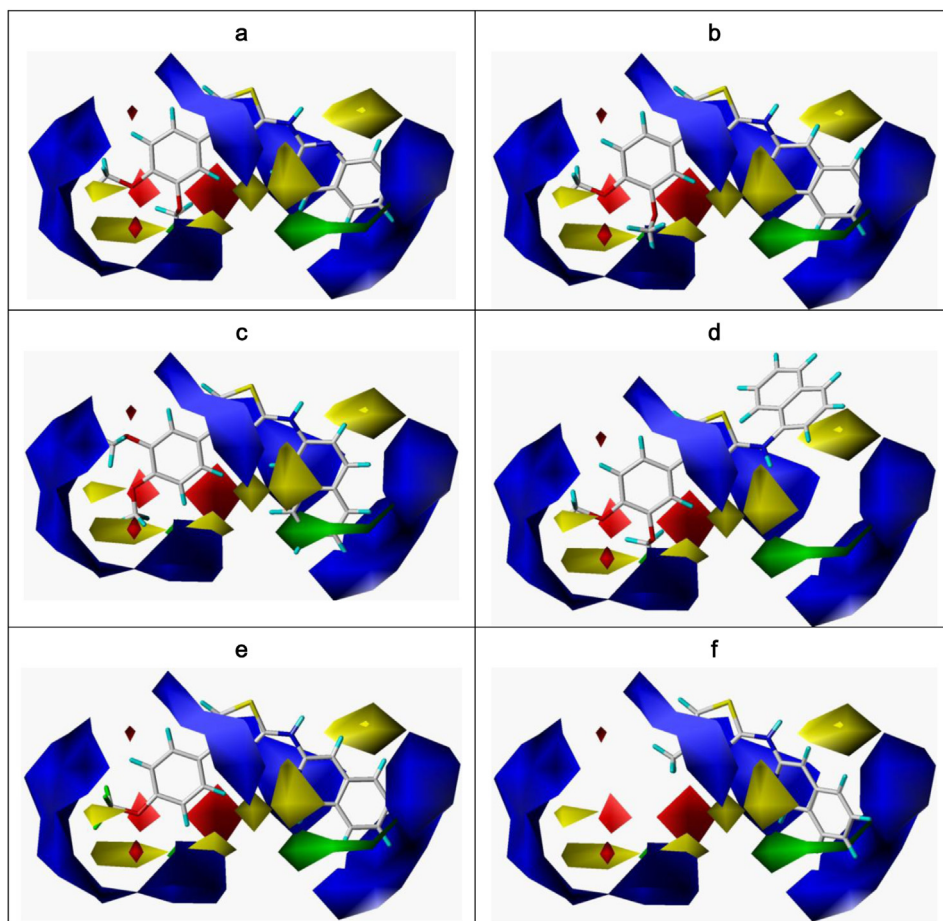
Fig. 3. Stereo view of CoMFA coefficient contours (STDEV*COEFF) for steric fields and electrostatic fields for most potent compounds a: **17**, b: **18**, c: **19** and less potent compounds d: **20**, e: **31** and f: **36** of 2-aminothiazoles. Steric fields: green contours indicate regions where bulky groups increase activity; yellow contours indicate regions where bulky groups decrease activity. Electrostatic fields: blue contours indicate regions where electropositive groups increase activity; red contours indicate regions where electronegative groups increase activity. (For interpretation of the references to color in this figure legend, the reader is referred to the web version of this article.)

maximum docking score of −14.7 kcal/mol, while other molecules showed the docking scores in the range between −8.8 and −14.7 kcal/mol, respectively. These results show that with decreasing EC_{50} values docking scores increased as shown in Table 3. A regression analysis of relative docking scores and $\Delta logEC_{50}$ values for 2-aminothiazole derivatives (see Table 3) was carried out and the scatter plots are drawn as shown in Fig. 5. From Fig. 5 it was found that the correlation coefficient of a relative docking score on the *X*-axis and $\Delta logEC_{50}$ values on the *Y*-axis for 2-aminothiazoles are 2.15 ($S = 0.3, F = 247.7$ where *S* is the standard error of the estimate and F is the significance of the regression) with an R^2 value of 0.71 (see Fig. 5). A good level of correlation (R^2 of 0.71) was obtained with SHaPrP model 6 between the docking scores and experimentally determined EC_{50} values for 30 compounds out of 37 compounds used in this study. Thus only model 6 of SHaPrP was taken for further docking studies with anti-prion compounds and other models were eliminated. The results also confirm that all these molecules bind to pocket D of SHaPrP and inhibit protein conversion from PrP^C to PrP^{Sc} [15]. Ligand protein interactions reveal that compound **17** (N-[4-(3,4-dimethoxyphenyl)-1,3-thiazol-2-yl]quinolin-2-amine) shows eight hydrophobic contacts with an interaction energy of −14.7 kcal/Mol. The oxymethyl ring of this compound orients towards the surface of the pocket and shows contacts with the backbone nitrogen of Asn197, and Cβ of Phe198 with two water molecules in the vicinity of the binding pocket while the quinoline moiety makes four hydrophobic contacts with Met134 (Cε), Met154

(Cβ), Ile205 (Cγ2) and Val209 (Cγ2) in the deeper side of the binding pocket. The thiazole group shows two hydrophobic contacts with Ile184 (Cγ2) and Met206 (Cβ) (see Fig. 6a). Replacing quinolin-2-amine with isoquinolin-3-amine allows the compound **18** (N-[4-(3,4-dimethoxyphenyl)-1,3-thiazol-2-yl]quinolin-2-amine) to bind with a lower interaction energy of −12.6 kcal/Mol (see Fig. 6b). In this binding orientation, isoquinolin-3-amine interaction shows the same hydrophobic contacts like quinolin-2-amine of compound **17**, while the oxymethyl ring of this compound slightly orients away from Asn197 and shows two hydrophobic contacts with Phe198 (Cβ) on the surface of the binding pocket and Met206 (Cβ) on helix-3. The oxymethyl ring also interacts with two water molecules through hydrogen bonds. Due to this orientation, the thiazole group interacts with Ile184 and Val210 instead of Met206. The nitrogen atom of isoquinolin-3-amine when replaced with carbon atom orients the naphthalene group of compound **19** (4-(3,4-dimethoxyphenyl)-N-(naphthalen-2-yl)-1,3-thiazol-2-amine) towards the surface of the pocket and shows contacts with Phe198 and Met206 through hydrophobic contacts (see Fig. 6c). The oxymethyl group penetrates deeper into the binding pocket showing three hydrophilic contacts with Met154, Ile205 (Cγ2) and Val209 (Cγ2). The oxymethyl ring also interacts with one of the water molecule in the vicinity through a hydrogen bond. Replacing 1-napthyl with 2-napthyl group allows the compound **20** (4-(3,4-dimethoxyphenyl)-N-(naphthalen-1-yl)-1,3-thiazol-2-amine) to bind with the same orientation as compound **18** expecting that the oxymethyl group
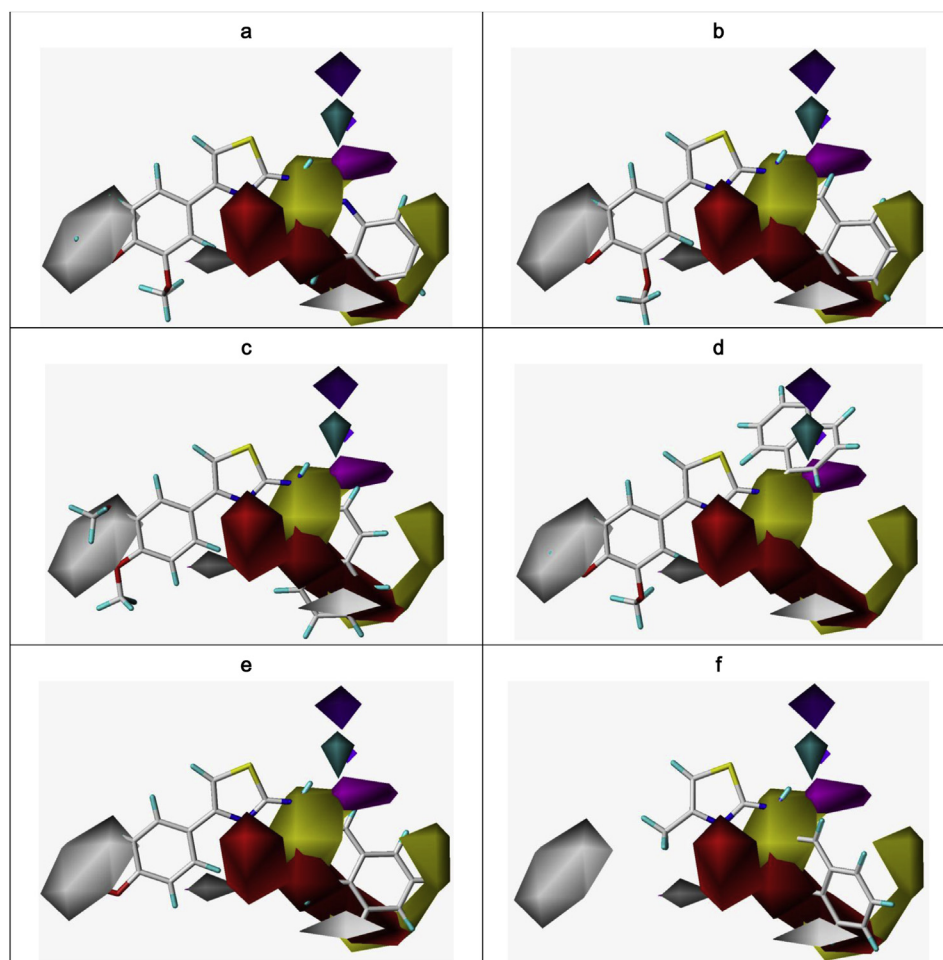
Fig. 4. Stereo view of CoMSIA coefficient contours (STDEV*COEFF) for steric, electrostatic, hydrophobic, donor and acceptor fields for most potent compounds a: **17**, b: **18** and c: **19** and less potent compounds d: **20**, e: **31** and f: **36** of 2-aminothiazoles. Yellow contour indicates hydrophobic groups are favorable, white contour indicates hydrophobic groups are unfavorable, green contour indicates region where bulky group increases activity Magenta contour indicates H-bond acceptor groups enhance binding affinity, whereas red contour decrease binding affinity. (For interpretation of the references to color in this figure legend, the reader is referred to the web version of this article.)
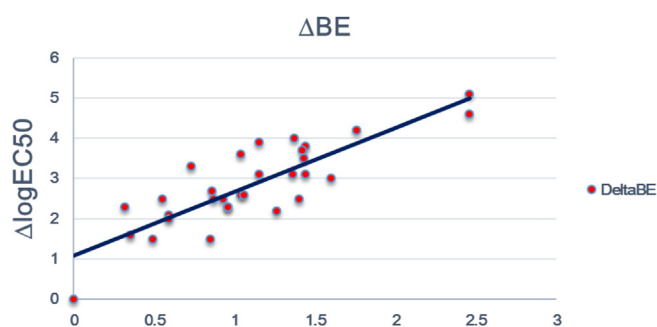

Fig. 5. Scatter plot of experimental EC$_{50}$ and docking scores for 2-aminothiazoles.

shows only one hydrophobic contact with Phe198 with an interaction energy of −12.0 kcal/Mol (see Fig. 6d). Replacing N-[4-(3,4-dimethoxyphenyl) group of compound **18** with N-{4-[4-(trifluoromethoxy)phenyl] and methyl groups allows compounds **31** (N-{4-[4-(trifluoromethoxy)phenyl]-1,3-thiazol-2-yl}isoquinolin-3-amine) and **36** (N-(4-methyl-1,3-thiazol-2-yl)isoquinolin-3-amine) to interact with an almost identical interaction energy of −8.6 and −8.7 kcal/Mol (see Fig. 6e and f). In these two compounds 1,3-thiazol-2-yl}isoquinolin-3-amine and isoquinolin-3-

amine were placed inside the pocket while N-{4-[4-(trifluoromethoxy)phenyl and N-(4-methyl) groups were exposed to the solvent. These orientations allow isoquinolin-3-amine of compound **31** to interact the same way as compound **17** with four hydrophobic contacts with Met134 (Cε), Met154 (Cβ), Ile205 (Cγ2) and Val209 (Cγ2) while the same group in compound 36 shows two hydrophobic contacts with Phe198 and Met206. These observations show that the electronegative nitrogen plays an important role in placing quinolin and isoquinolin groups of these compounds deeper into the binding pocket of SHaPrP. The results also reveal an important information that all these inhibitors bind to pocket-D of SHaPrP without breaking the salt bridge between Arg156 and Glu196 as shown in Fig. 8.

2.4. Docking versus CoMFA and CoMSIA

The overlay of CoMFA steric and electrostatic contour maps on the compound 17 is shown in Fig. 3. These contour maps were compared and contrasted with the docking orientations in the binding site of SHaPrP. Previous reports also reveal the advantages of such comparisons using a unified pharmacophore model [16]. The green contours near the nitrogen atom of quinoline and isoquinoline groups fall in the hydrophobic pocket-D formed between helix-2 and helix-3. The aliphatic side chains of Phe198, Ile184,

Table 3
Calculated binding energies of 2-amino thiazoles predicted using MOE.

Comp	EC$_{50}$ (mM)	Log EC$_{50}$	ΔLog	BE	ΔBE
4	3.01	3.47	1.43	−11.2	3.5
5	32	4.5	2.46	−9.6	5.1
6	8.2	3.91	1.87	−14.3	0.4
7	1.22	3.08	1.04	−11.1	3.6
8	28	3.44	1.4	−12.2	2.5
9	6.38	3.8	1.76	−10.5	4.2
10	3.94	3.59	1.55	−13.9	0.8
11	15.6	3.19	1.15	−11.6	3.1
12	2.53	3.4	1.36	−11.6	3.1
13	1	3	0.96	−12.4	2.3
14	0.79	2.89	0.85	−13.2	1.5
15	7.29	3.86	1.82	−13.1	1.6
16	1	3	0.96	−12.4	2.3
17	0.11	2.04	0	−14.7	0
18	0.43	2.63	0.59	−12.6	2.1
19	0.39	2.59	0.55	−12.2	2.5
20	32	4.5	2.46	−12	2.7
21	3.03	3.48	1.44	−10.9	3.8
22	29	3.46	1.42	−11	3.7
23	1.57	3.19	1.15	−10.7	4
24	0.86	2.93	0.59	−10.7	4
26	1.23	3.08	1.04	−12.1	2.6
27	0.94	2.97	0.93	−12.2	2.5
30	0.34	2.53	0.49	−13.2	1.5
31	32	4.5	2.46	−13.5	1.2
32	0.31	2.49	0.45	−10.3	4.4
33	3.08	3.48	1.44	−11.6	3.1
34	2.01	3.3	1.26	−12.5	2.2
35	0.8	2.9	0.86	−12.0	2.7
36	32	4.5	2.46	−10.1	4.6
40	0.23	2.36	0.32	−12.4	2.3
41	0.25	2.39	0.35	−13.1	1.6
42	0.6	2.77	0.73	−11.4	3.3
43	1.27	3.1	1.06	−12.1	2.6
44	0.82	2.91	0.87	−12.2	2.5
45	4.42	3.64	1.6	−11.7	3
47	8.18	3.91	1.87	−13.1	1.6

Ile205, Val209, and Val210 lining the hydrophobic pocket make contacts with quinoline and isoquinoline groups. This indicates that substituents that combine both electronegative and lipophilic properties are preferred at these positions. Thus, the results of CoMFA, CoMSIA and docking studies validate each other and indicate the importance of the binding step in overall drug action. These results imply that the presence of the oxymethyl groups in meta and para positions on the phenyl ring is necessary for activity, and an electro-negative nitrogen is highly favorable to enhance activity. In summary, contour maps generated by CoMFA and CoMSIA provide valuable information to understand the 3D-QSAR relationship between the structures and their biological activities. The results of CoMFA, and CoMSIA are in good agreement with our docking studies which indicates that the results are highly reliable. The field properties of the CoMFA and CoMSIA not only coincide with the pharmacophore features of the binding mode but also help to predict the pharmacophores of the new drugs and their activity prior to synthesis.

2.5. Virtual screening and docking studies of new antiprion compounds

The pharmacophoric model that was generated from GALAHAD was used further for virtual screening of ligands using the MOE chemical database. In total, 150 hit compounds were selected by applying a maximum fit value of 85. Out of the 150 compounds, six compounds with different scaffolds were chosen for molecular docking and experimental analysis against SHaPrP (see Table 4). Blind docking studies allow these six compounds to bind to pocket-D of

SHaPrP with an overall good H-bond and hydrophobic interactions. The 4-methylpyrimidin-2-amine group of compound **1** ((5-(3, 4-dimethoxyphenyl)-4-methylpyrimidin-2-amine)) (Bionet 1G-037) enters deeper into the pocket while dimethoxy-phenyl group occupies the surface area and shows hydrophobic contact with Phe198 with the interaction energy of −9.4 kcal/mol (see Fig. 7a). Removal of 4-oxymethyl group from 5-(3,4-dimethoxyphenyl) group and replacing 4-methyl with 4-methoxy phenyl in compound **1** allows compound **2** (5T-0214) to bind with a higher interaction energy of −10.8 kcal/mol (see Fig. 7b). The 4, 5-bis (4-methoxyphenyl) pyrimidin-2-amine occupies the surface of the binding pocket showing a hydrophobic contact with Phe198 while 2-amine acts as a proton donor and Tyr149 acts as a proton acceptor. The oxygen atom of 4-methoxyphenyl interacts with Arg156 though water mediation. Replacing pyrimidin-2-amine of compound **2** with 1, 3-thiazole-2-amine group (compound **3**)(Bionet 6T-0265) allows the molecule to form a hydrophobic contact with Phe198 with a higher interaction energy of −12.1 kcal/mol (see Fig. 7c). Additionally, the molecule also shows hydrogen bonding with two water molecules in the vicinity of the binding site. In this orientation, methoxy phenyl group attached to the fifth position of 2-amino-1, 3-thiazole moiety shows hydrogen bonding interaction with a water molecule in the deeper part of the binding site while methoxy phenyl attached to the fourth position shows hydrogen bonding with the water molecule on the surface of the binding site. The 2-amine group attached to 1, 3-thiazole shows water mediate interaction with Arg148 near the end of the helix-1. Modification of compound **3** by removal of 4-methoxyphenyl and addition of a methoxy group in the second position of 5-methoxyphenyl allows compound **4** (Chembridge 6413213) to interact with the same affinity and a binding energy of −12.1 kcal/mol (see Fig. 7d). The 1, 3 thiazole shows a hydrogen Pi-interaction with Arg156 while the 2-amino group acts as a proton donor and Gly195 acts as a backbone acceptor. Attaching 3, 4, 5-trimethoxybenzamide to 4-(2, 5-dimethoxyphenyl)-5-methyl-1, 3-thiazol-2-amine of compound **4** allows compound **5** ((4-(2, 4-dimethoxyphenyl)-5-methyl-1, 3-thiazol-2-amine) (Chembridge 6872366) to bind with a lower interaction energy, namely −11.5 kcal/mol (see Fig. 7e). The 2,4-dimethoxyphenyl group of compound **5** orients into the binding pocket and shows hydrophobic contact with Phe198, while 5-methyl-1,3-thiazol-2-amine shows one hydrogen bond with Gly195 on the surface of the binding pocket. The oxygen atom of the 2-4-dimethoxyphenyl group shows a water-mediated interaction with Asn197 on the loop between helix-2 and helix-3. The oxygen atoms of 3,4,5 trimethoxy phenyl group shows two-water mediated interactions with Tyr162, Gln186 and Thr190 of SHaPrP. This compound is very similar to one of the known compound (compound **21**) of 2-aminothiazole expect the addition of oxymethy group in the 4 position of phenyl group. Because of its similarity this compound can be treated as a positive control for experimental analysis. Finally, compound **6** (3-{5-[(2, 5-dimethoxyphenyl) amino]-1,3,4-thiadiazolidin-2-yl}-5,8-methoxy-2H-chromen-2-one) (Chembridge 6623338) binds with a high interaction energy of −13.2 kcal/mol compared to other five compounds studied (see Fig. 7f). 8-methoxy-2H-chromen-2-one group penetrates very deep into the pocket while 1, 4-dimethoxybenzene is placed very near to the surface showing five hydrophobic contacts with Cγ of Met134, Cδ2 of Phe198, Cε of Met206 and Cγ2 Val209. The thiazolidin group shows a hydrogen−Pi interaction with Tyr157 on the loop between helix-1 and beta-2 of SHaPrP. These docking results of 2-aminothiazoles and new antiprion compounds show that Met134 in loop1 between β1 and α1, Tyr149 in α1, Met154, Arg156 and Tyr157 in loop2 between α1 and β2, Ile184 in α2, Gly195, Asn197 and Phe198 in loop3 between α2 and α3, and Ile205, Met206, Val209 and Val210 residues in α3 act as common pharmacophores of these compounds preventing the prion conversion to pathogenic form from PrP^C to PrP^{Sc} (see Fig. 8). These results also
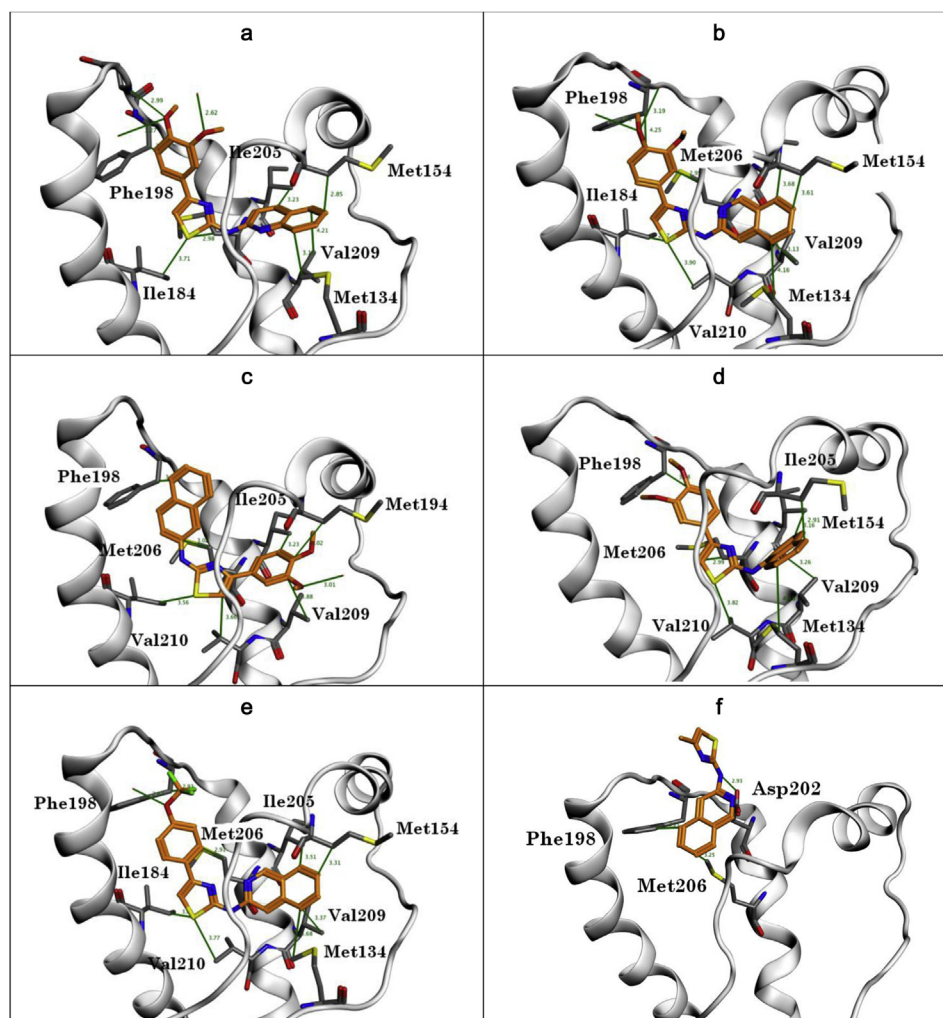
Fig. 6. Binding modes of most potent compounds a: **17**, b: **18**, c: **19** and less potent compounds d: **20**, e: **31** and f: **36** against ShPrP.

suggest that the residues of H2H3 play an important role in the binding orientations of these compounds with pocket-D of SHaPrP. The orientations of these compounds further stabilize the salt bridge between Arg156 and Glu196, which play an important role in prion conversion from PrP^C to PrP^{Sc}. Previous NMR studies also reveal that the known compound GN8 interacts with N159 in loop2 and E196 in loop3 through hydrogen bonds and significantly prohibits large conformational changes, which further blocks the formation of PrP^{Sc} or PrP^U [13]. Structural studies also indicated that the side chains of Thr183 and Phe198 contribute to interactions between secondary structure elements and stabilize the hydrophobic core of the C-terminal globular domain of PrP^C [17]. Site directed mutagenesis of Phe198Ser undergoes a time-dependent conversion to oligomeric structures that are ThT-positive and morphologically appear similar to those found in the brain tissue of GSS patients [18]. The residue Met134 is highly exposed to the solvent and is easily oxidized. This residue along with Met109, 112, 129, and 134 are located in a region which is critical for the conversion of PrP^C to pathogenic form PrP^{Sc}. Oxidation of Met134 might introduce structural strains resulting in increased PrP instability [19,20]. The data also demonstrate that thermodynamic stability of PrP^C is greatly increased by the mutation of Val209Met resulting in a remarkably reduced propensity of the protein to undergo a conversion to PrP^{Sc} mimicking, β-sheet-rich aggregates *in vitro* [21]. Previous MD studies on human PrP have also revealed a significant loss of α-helical content of H2 followed by H3 at
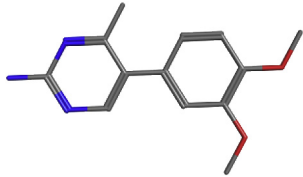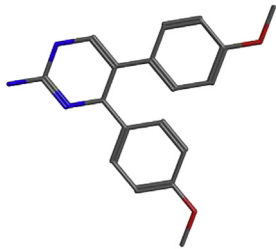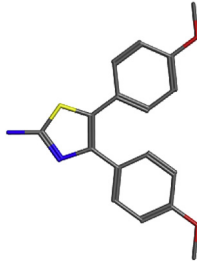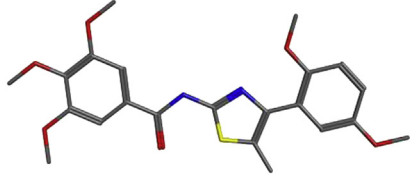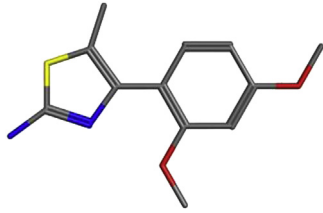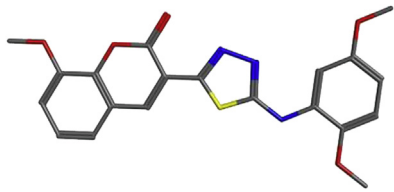
low pH combined with high temperature [22—24]. Coarse grained protein MD simulation of the CJD-causing T183A variant also showed that H2 and H3 display a high propensity for intra- and inter-β-sheets [25]. Previous studies using chromatography and light scattering on ovine PrP (OvPrP) has demonstrated that H2H3 domain has a higher polymerization rate compared to the full-length construct. Furthermore, the depolymerization kinetics of purified H2H3 oligomers reveal that regions outside H2H3 do not significantly contribute to the oligomerization process compared to those purified from the full-length PrP [26]. Hydrogen/deuterium exchange and introduction of disulfide bonds also revealed that before oligomerization, separation of contacts in the globular part (residues 127—234) occurred between the S1—H1—S2 domain (residues 132—167) and the H2—H3 bundle (residues 174—230), implying a conformational change of the S2—H2 loop (residues 168—173) [27]. In addition, the involvement of glycosylation of H2 in PrP^C (N184 and N200, sheep numbering) could also have an effect on the polymerization process [28].

2.6. Fluorescence quenching study of new antiprion compounds

The interaction of new antiprion compounds with SHaPrP was investigated using fluorescence emission spectra to determine the binding site similar to the computationally predicted binding site. Prion protein has one tryptophan residue, Trp145 which shows intrinsic fluorescence. Changes in the emission spectra of the prion

Table 4
Binding energies of new antiprion compounds identified by virtual screening using MOE database.

Comp	Structure	Name of the compound	Binding energy	K_d (μM)
1		Bionet 1G-037	−9.4	384
2		Bionet 5T-0214	−10.8	57.8
3		Bionet 6T-0265	−12.1	15.5
4		Chembridge 6413213	−11.5	185
5		Chembridge 6872366	−12.1	84.7
6		Chembridge 6623338	−13.2	44.14

protein were monitored at 350 nm upon titration of the ligand onto protein due to conformational changes. The maximum emission of fluorescence spectra at 350 nm suggests that the tryptophan residue is highly exposed on the surface of the SHaPrP. A shift in λmax from 310 to 350 nm towards higher wavelengths (red shift) was observed when the prion protein was titrated with the compounds **2**–**4** and **6**, respectively. This red shift in λmax is likely to indicate

the presence of these antiprion compounds in the vicinity of Trp145. These observed spectral changes and the shift in the position of λmax of SHaPrP are likely to reflect direct and indirect interactions of these antiprion compounds with the hydrophobic and hydrophilic regions located in the vicinity of Trp145 and to reflect induced conformational changes. These spectral changes reflect a purely static quenching process that would exhibit a good
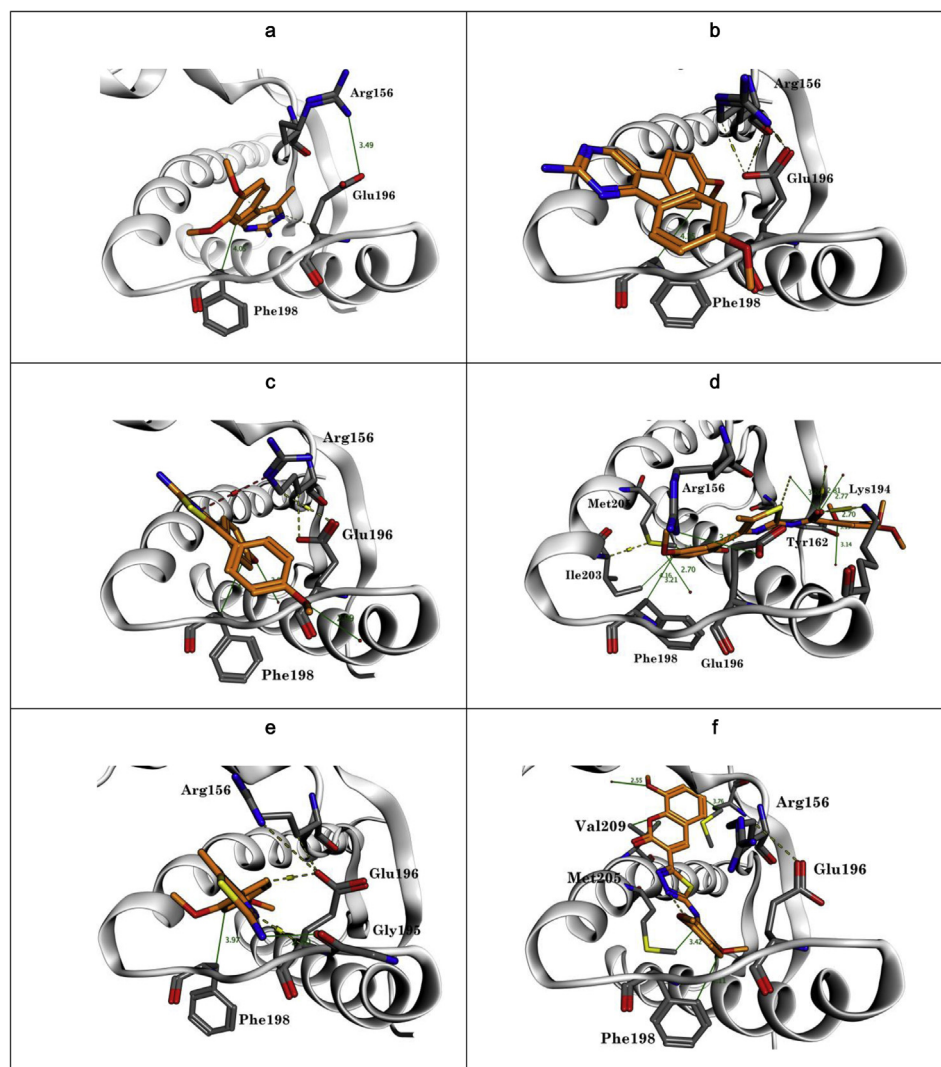
Fig. 7. Binding modes of virtual screened compounds a: **1**, b: **2**, c: **3**, d: **4**, e: **5** and f: **6** in the binding pocket-D of SHaPrP.

linear relationship. According to the results illustrated in Fig. 9a–d, a linear relation of $(F_0/F) - 1$ indicates a static quenching process in SHaPrP. The changes in fluorescence intensity were plotted according to Equation and binding constant values for these compounds were estimated as shown in Table 4. Linear regression analyzed in Fig. 9a–d revealed that the ligand–protein complex is driven by hydrophobic contacts of pocket-D with SHaPrP. Our fluorescence studies showed that compound **1** interacted with much lower affinity with a K_d value of 384 μM while compound **2** binds with an estimated K_d value of 88.5 μM. The compound **4** binds with intermediate affinity compared to compounds **1**, **2** and **5** with a binding constant value of 185 μM. Finally, the compound **3** which binds with higher affinity to SHaPrP, with an estimated binding constant (K_d) of 15.5 shows nonlinear regression compared to compound **6** which shows linear regression with a K_d value of 46.4 μM. These nonlinear and linear regression analyses clearly indicate that compound **3** also shows affinity towards binding pockets other than pocket-D while compound **6** binds only with pocket-D of SHaPrP. This reveals that compound **6** is the best antiprion compound compared to the other four compounds used in this study. Fluorescence titration also determined that the compound **5** used as a positive control binds to pocket-D similarly to the computationally predicted binding site with an estimated
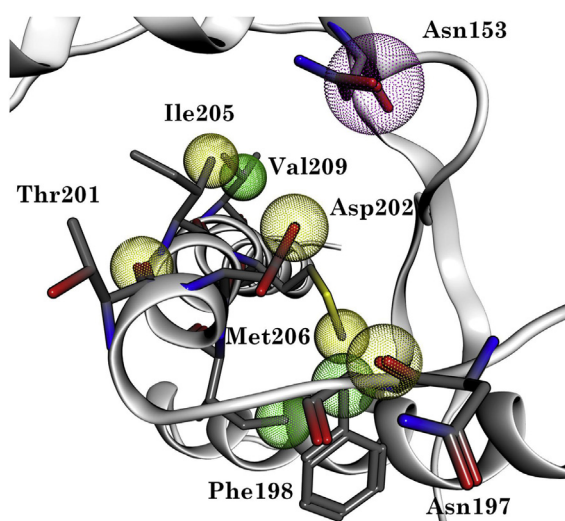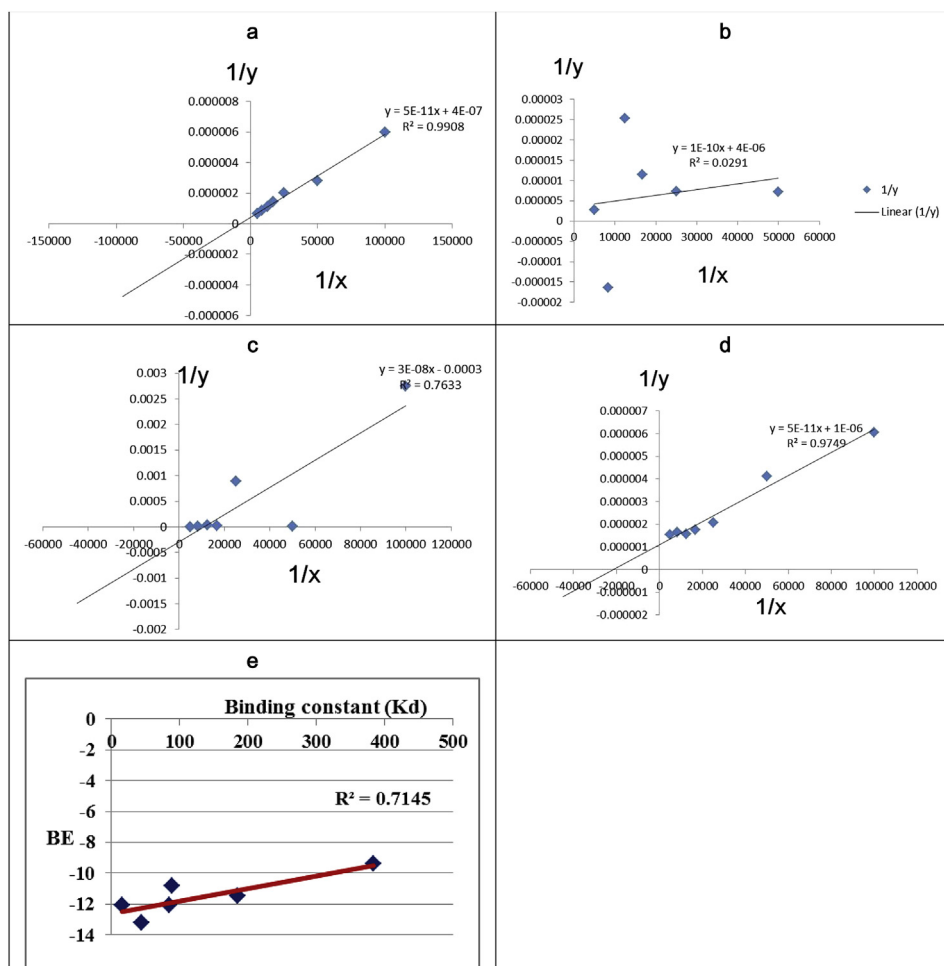

Fig. 8. Pharmacophore analysis of 2-aminothizoles, and virtually screened compounds that bind to pocket-D of SHaPrP.

$1/\Delta F = Y$

$1/[\text{LIGAND}] = X$

INTERCEPT ON X= -1/Kd

Fig. 9. Titration curves for the new antiprion compounds a: **2**, b: **3**, c: **4** and d: **6** analyzed using flourescencing binding assay. e: Scatter plot of experimental K_d values and docking scores for new antiprion compounds.

binding constant (K_d) of 84.7 µM. A regression analysis of docking scores and K_d values for these new antiprion compounds (see Table 4) was carried out and scatter plots are drawn as shown in Fig. 9e. From Fig. 9e it was found that the docking scores for these new antiprion compounds showed a good level of correlation with experimental binding constant (K_d) values with an R^2 value of 0.71.

2.7. Negative control

Since all the compounds of 2-aminothiazoles and virtually screened compounds bind to pocket-D of SHaPrP, the known compound noscapine taken as negative control was docked against SHaPrP and its binding site was predicted. The docking studies showed that noscapine binds on the surface of the pocket-A at the "rigid loop" (the region comprising residues NNQNNF located between β2 and α2) with two hydrogen bond interactions with Arg164 and this might disturb the salt bridge interaction with Asp178 (see Fig. 10a and b). Furthermore, the interaction of noscapine with SHaPrP was investigated using fluorescence titration to determine the binding of noscapine similarly to the computationally predicted binding site. The fluorescence

quenching of tryptophan can be monitored by emission intensity at 350 nm upon titration of the ligand onto proteins. A purely static quenching process would exhibit a good linear relationship. According to the results illustrated in Fig. 10c, a nonlinear relation of $(F_0/F) - 1$ indicates a non-static quenching process in SHaPrP. The changes in fluorescence intensity were plotted according to Equation and binding constant values for noscapine were estimated. Nonlinear regression analyzed in Fig. 10c revealed that the ligand–protein complex is driven by polar interactions near the rigid loop of SHaPrP. Our fluorescence studies showed that noscapine interacted less strongly with SHaPrP, with an estimated binding constant (K_d) of 29 µM. These studies using computational and experimental methods reveal that noscapine might act as an accelerator for prion propagation from PrP^C to PrP^{Sc}. Previous experimental studies have also shown that Asp178 shows hydrogen bonding interaction with Arg164 in the wild-type prion protein [29]. It has been proposed that the pathologically relevant mutant Asp178Asn (D178N) might destabilize the structure of the prion protein because of the loss of the Arg164-Asp178 salt bridge. Furthermore, experimental studies on D178N point mutation when PrP^C is expressed in the cytosol found it to remarkably and
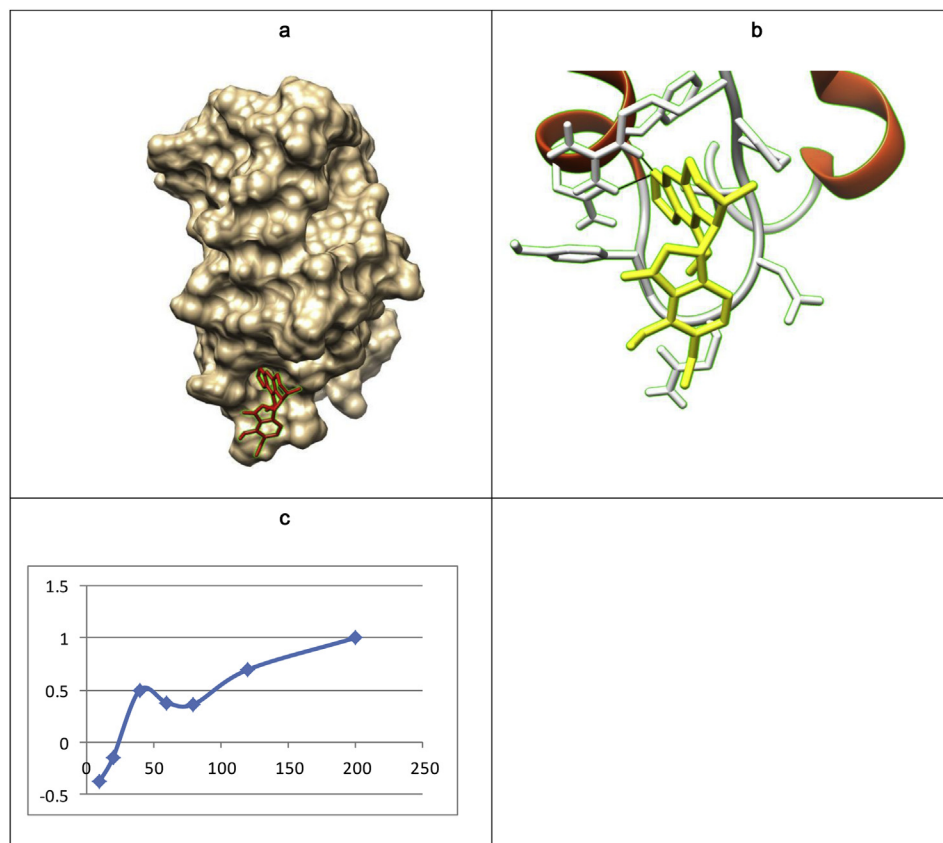
Fig. 10. Surface representation of SHaPrP with the binding mode of a: noscapine. b: interaction of noscapine with the pocket-A of SHaPrP. c: Titration curve of noscapine monitored by florescence spectroscopy.

specifically enhance PrP^C conversion to PrP^{Sc}-like isoforms [30]. Moreover, in an acidic environment where Asp178 is expected to be protonated and hence unable to bind effectively with Arg164 and Tyr128 side chains as in the D178N mutant, PrP^{Sc}-like aggregates are spontaneously formed. But molecular dynamics simulations of the prion mutant D178N suggest that the salt bridge between Arg164 and Asp178 might not be crucial for the stability of the prion protein due to minor deviations from the folded conformation [31].

3. Conclusions

In this study, we have successfully combined the CoMFA, and CoMSIA methods to build 3D-QSAR models for prion inhibitors. The good correlation obtained between the experimental and predicted pEC$_{50}$ values indicated that all the generated models in our study are stable and robust. The results of CoMFA/CoMSIA field maps provide useful information to optimize the thiazole class of derivatives. A good correlation between binding energies and the experimentally determined EC$_{50}$ with an R^2 value of 0.78 reveals that all these molecules bind to pocket-D of SHaPrP maintaining the salt bridge between Arg156 and Glu196. Virtual screening of the compounds using pharmacophoric model identified five new compounds with anti-prion activity. Experimental studies using fluorescence quenching also show that these compounds bind to pocket-D of SHaPrP near Trp145. The compounds **3** and **6** exhibit a significant anti-prion effect with higher binding constant (K_d) values of 15.5 and 46.4 μM, respectively, compared to other compounds used in this study. Molecular docking and fluorescence quenching also show that noscapine binds on the surface of pocket-

A near the rigid loop of SHaPrP interacting with Arg164 which is involved in the salt bridge interaction with Asp178. Thus, this study clearly demonstrates the importance of pocket-D for the development of antiprion drugs in prion inhibition from PrP^C to PrP^{Sc}. These results also indicate that our computational predictions show very good correlation with experimental data. The evaluation of these compounds in animal models of prion disease will be of significant interest.

4. Methodology

A series of potent anti-prion compounds (37-2-aminothiazoles) whose EC$_{50}$ was measured, have been identified from the literature [14]. The compounds were randomly divided into a training set ($n = 32$) and a test set ($n = 5$). The test set molecules (compounds **15**, **17**, **19**, **20** and **31**) were selected manually to cover low, middle, and high biological activity of the dataset. The ligands were built and optimized with all hydrogens using SYBYL-X 1.3 (Tripos Associates Inc.) using the force field "Tripos" with Gasteiger-Marsili atomic partial charges [32,33]. The EC$_{50}$ values (i.e., the concentration of an inhibitor that produces 50% inhibition of prion activity) were converted into pEC$_{50} = -$logEC$_{50}$. The structures and biological activities of all compounds are represented graphically (see Fig. S1). To generate reliable QSAR models in CoMFA and CoMSIA all compounds were aligned using the GALAHAD feature-based pharmacophore prediction software [34]. The structural elements of each compound bound to the biological activity were flexibly aligned using different torsional degrees of freedom [35]. The pharmacophore-based molecular alignment generated a rationale for CoMFA studies with default settings [36]. Five physico-

chemical properties (electrostatic, steric, hydrophobic, and hydrogen bond donor and acceptor) were evaluated using a common probe atom placed within a 3D grid using CoMSIA [37]. The linear correlation between the CoMFA and CoMSIA fields and the biological activity values were explored using the partial least squares (PLS) method [38]. Initially, the leave-one-out (LOO) cross-validation method was conducted to determine the number of components and cross-validation coefficient, q^2 [39]. To determine the sensitivity of the model and address the issue of false sense of confidence, the progressive scrambling method was used to test the model stability [40,41]. To derive the final PLS model, the optimum number of components was used with no validation method [42,43]. These compounds were further docked against the represented models (models 1, 6 10 and 17 of the original NMR ensemble) of SHaPrP [15]. In order to identify a suitable prion (PrP^C) structural model for docking, the NMR structures of the Syrian hamster prion protein, ShPrP (1B10.pdb), were superposed and grouped into four different clusters using the first model as a template. For each cluster, one representative model (models 1, 6 10 and 17 of the original NMR ensembles) was chosen [15]. Hydrogen atoms were added and the structures further minimized with the CHARMM27 force field [44] using the generalized Born implicit solvent representation until the energy gradient was less than 0.05 kcal/Mol [37,42]. To take into account a possible role of bound water molecules in ligand binding, the 105 water coordinates from the X-ray structure of the Human prion protein, HuPrP (3HAK.pdb), were transferred to our representative model and energy minimized. The alpha carbon RMSD between the HuPrP and shPrP is 2.7Å. The same force field and energy minimization protocol described above was used to confirm proper solvent layer placement and resolve any van der Waal's violations. MOE's alpha site finder was used to identify potential ligand binding pockets on the protein. In total, four regions of the protein were identified as potential pockets [15]. For *in-silico* docking of ligands onto the target protein the ligand placement method in MOE called "Alpha PMI" was employed to bias the conformational search of the ligand to meaningful trials. In all cases, the London ΔG method was used for scoring and the TAFF force field was used for energy minimization [32]. The binding site side chains were constrained using a force constant of 1.0 kcal/Mol Å^2. The final docking poses were ranked according to the interaction energies (U_{total} in kcal/mol) as the sum of electrostatic and van der Waals energies and the flexibility of the ligand itself using the London ΔG scoring function. The pharmacophoric model that was generated using GALAHAD was used as a scaffold for virtual screening [45]. In this study, five compounds from the training set, whose functional R groups are matching well the molecular fields suggested by the CoMFA or CoMSIA models to be important for activity, were selected to generate pharmacophore models. The compounds identified using virtual screening were used for further blind docking studies. Pharmacophore analysis for the docked conformations of new antiprion compounds was predicted using MOE software which is a set of structural features of the ligand that are directly related to the ligand's recognition at a receptor site and its biological activity. Each ligand conformation is assigned a set of annotation points, which is a set of structural features that may contribute to the ligand's pharmacophore. A database of conformations can be searched with a query that represents a pharmacophore hypothesis. The result of such a search is a set of matches that align the pharmacophoric features of the query to the pharmacophoric features present in the ligands of the searched database. Finally, fluorescence spectra of new antiprion compound were collected on a PTI MODEL-MP1 spectro-fluorimeter using a 10 mm path length cell. Spectral data were collected using fluorescence software and data analysis was performed using OriginPro® 7.5 software (OrginLab®, North-ampton, MA, USA). For all the experiments an excitation wavelength of 350 nm and a scan range of 350–600 nm were used. Steady-state fluorescence of compound **6** was measured by fixing the ligand concentration at 20 μM and adding incremental aliquots (10–140 μM) of the protein in phosphate buffer at pH 7 and the fluorescence enhancement data was used to determine the apparent binding constant according to Equation [46]

$$1/\Delta FI = 1/\Delta FImax + 1/(Kb\Delta FImax[Prt])$$

where ΔFI is the change in the ligand fluorescence intensity in the presence of the protein, $\Delta FImax$ is the maximal change in fluorescence intensity, Kb is the binding constant, and $[Prt]$ is the concentration of the protein added.

Appendix A. Supplementary data

Supplementary data related to this article can be found at http://dx.doi.org/10.1016/j.ejmech.2014.07.045.

References

[1] S.B. Prusiner, Novel proteinaceous infectious particles cause scrapie, Science 9 (1982) 136–144.

[2] S.B. Prusiner, Prions, Proc. Natl. Acad. Sci. U. S. A. 95 (1998) 13363–13383.

[3] D.A. Kocisko, G.S. Baron, R. Rubenstein, J. Chen, S. Kuizon, B. Caughey, New inhibitors of scrapie associated prion protein formation in a library of 2000 drugs and natural products, J. Virol. 77 (2003) 10288–10294.

[4] V. Perrier, A.C. Wallace, K. Kaneko, J. Safar, S.B. Prusiner, F.E. Cohen, Mimicking dominant negative inhibition of prion replication through structure-based drug design, Proc. Natl. Acad. Sci. U. S. A. 97 (2000) 6073–6078.

[5] A. Kimata, H. Nakagawa, R. Ohyama, T. Fukuuchi, S. Ohta, K. DohUra, T. Suzuki, N. Miyata, New series of anti-prion compounds: pyrazolone derivatives have the potent activity of inhibiting protease resistant prion protein accumulation, J. Med. Chem. 50 (2007) 5053–5056.

[6] I. Yudovin-Farber, T. Azzam, E. Metzer, A. Taraboulos, A.J. Domb, Cationic polysaccharides as antiprion agents, J. Med. Chem. 48 (2005) 1414–1420.

[7] K.T. Doh-ura, B. Iwaki, Caughey lysosomotropic agents and cysteine protease inhibitors inhibit scrapie-associated prion protein accumulation, J. Virol. 74 (2000) 4894–4897.

[8] R. Lüllmann-Rauch, R. Pods, B. von Witzendorff, The antimalarials quinacrine and chloroquine induce weak lysosomal storage of sulphated glycosaminoglycans in cell culture and in vivo, Toxicology 110 (1996) 27–37.

[9] M.S. Vogtherr, B. Grimme, D.M. Elshorst, K. Jacobs, C. Fiebig, R. Grie-singer, R. Zahn, Antimalarial drug quinacrine binds to C-terminal helix of cellular prion protein, J. Med. Chem. 46 (2003) 3563–3564.

[10] C. Korth, B.C. May, F.E. Cohen, S.B. Prusiner, Acridine and phenothiazine derivatives as pharmacotherapeutics for prion disease, Proc. Natl. Acad. Sci. U. S. A. 98 (2001) 9836–9841.

[11] I. Murakami-Kubo, K. Doh-ura, K. Ishikawa, S. Kawatake, K. Sasaki, J. Kira, S. Ohta, T. Iwaki, Quinoline derivatives are therapeutic candidates for transmissible spongiform encephalopathies, J. Virol. 78 (2004) 1281–1288.

[12] B. Caughey, W.S. Caughey, D.A. Kocisko, K.S. Lee, J.R. Silveira, J.D. Morrey, Prions and transmissible spongiform encephalopathy (TSE) chemotherapeutics: a common mechanism for anti-TSE compounds, Acc. Chem. Res. 39 (2006) 646–653.

[13] K. Kuwata, N. Nishida, T. Matsumoto, O. Yuji, K. Junji, H. Muto, K. Kodama, K. Hironori, K. Nakamura Kimura, M. Kawasaki, Y. Takakura, S. Shirabe, J. Takata, Y. Kataoka, S. Katamine, Hot spots in prion protein for pathogenic conversion, PNAS 104 (2007) 11921–11926.

[14] Alejandra Gallardo-Godoy, Joel Gever, Kimberly L. Fife, B. Michael Silber, Stanley B. Prusiner, Adam Renslo, 2-Aminothiazoles as therapeutic leads for prion diseases, J. Med. Chem. 54 (2011) 1010–1021.

[15] Nataraj S. Pagadala, Trent C. Bjorndahl, Nikolay Blinov, Andriy Kovalenko, David S. Wishart, Molecular docking of thiamine reveals similarity in binding properties between the prion protein and other thiamine-binding proteins, J. Mol. Model. 19 (2013) 5225–5235.

[16] (a) W. Sippl, H.D. Holtje, J. Mol. Struct. (Theochem) 503 (2000) 31;
(b) J.K. Buolamwini, H.J. Assefa, Med. Chem. 45 (2002) 841–852;
(c) G.R. Desiraju, B. Gopalakrishnan, R.K.R. Jetti, A. Nagaraju, D. Raveendra, J.A.R.P. Sarma, R. Thilagavathi, M.E.J. Sobhia, Med. Chem. 45 (2002) 4847–4857.

[17] Sophia Kiachopoulos, Andreas Bracher, F. Konstanze Winklhofer, Jorg Tatzelt, Pathogenic mutations located in the hydrophobic core of the prion protein interfere with folding and attachment of the glycosylphosphatidylinositol anchor, J. Biol. Chem. 280 (2005) 9320–9329.

[18] G. Giaccone, L. Verga, O. Bugiani, B. Frangione, D. Serban, S.B. Prusiner, M.R. Farlow, B. Ghetti, F. Tagliavini, Proc. Natl. Acad. Sci. U. S. A. 89 (1992) 9349–9353.

[19] J.H. Viles, D. Donne, G. Kroon, S.B. Prusiner, F.E. Cohen, H.J. Dyson, P.E. Wright, Local structural plasticity of the prion protein, analysis of NMR relaxation dynamics, Biochemistry 40 (2001) 2743—2753.

[20] D. Peretz, R.A. Williamson, Y. Matsunaga, H. Serban, C. Pinilla, R.B. Bastidas, R. Rozenshteyn, T.L. James, R.A. Houghten, F.E. Cohen, S.B. Prusiner, D.R.A. Burton, A conformational transition at the N terminus of the prion protein features in formation of the scrapie isoform, J. Mol. Biol. 273 (1997) 614—622.

[21] Qingzhong Kong, Bishwajit Kundu, Xinyi Li, Liuting Qing, Krystyna Surewicz, Ignazio Cali, Shenghai Huang, Mengjie Zheng, Wieslaw Swietnicki, D. Frank Sönnichsen, Pierluigi Gambetti, K. Witold Surewicz, Cell Rep. 4 (2013) 248—254.

[22] W. Gu, T. Wang, J. Zhu, Y. Shi, H. Liu, Molecular dynamics simulation of the unfolding of the human prion protein domain under low pH and high temperature conditions, Biophys. Chem. 104 (2003) 79—94.

[23] E. Langella, R. Improta, V. Barone, Checking the pH-induced conformational transition of prion protein by molecular dynamics simulations: effect of protonation of histidine residues, Biophys. J. 87 (2004) 3623—3632.

[24] N. Blinov, M. Berjanskii, D.S. Wishart, M. Stepanova, Structural domains and main-chain flexibility in prion proteins, Biochemistry 48 (2009) 1488—1497.

[25] Y. Chebaro, P. Derreumaux, The conversion of helix H2 to beta-sheet is accelerated in the monomer and dimer of the prion protein upon T183A mutation, J. Phys. Chem. B 113 (2009) 6942—6948.

[26] Nesrine Chakroun, Stephanie Prigent, A. Cecile Dreiss, Sylvie Noinville, Celine Chapuis, Franca Fraternali, Human Rezaei, The oligomerization properties of prion protein are restricted to the H2H3 domain, FASEB J. 24 (2010) 3222—3231.

[27] Frederic Eghiaian, Thorsten Daubenfeld, Yann Quenet, Marieke van Audenhaege, Anne-Pascale Bouin, Guillaume van der Rest, Jeanne Grosclaude, Human Rezaei, Diversity in prion protein oligomerization pathways results from domain expansion as revealed by hydrogen/deuterium exchange and disulfide linkage, PNAS (2007) 7414—7419.

[28] W.P. Esler, E.R. Stimson, J.M. Jennings, H.V. Vinters, J.R. Ghilardi, J.P. Lee, P.W. Mantyh, J.E. Maggio, Alzheimer's disease amyloid propagation by a template-dependent dock-lock mechanism, Biochemistry 39 (2000) 6288—6295.

[29] R. Riek, G. Wider, M. Billeter, S. Hornemann, R. Glockshuber, K. Wuthrich, Prion protein NMR structure and familial human spongiform encephalopathies, Proc. Natl. Acad. Sci. U. S. A. 95 (1998) 11667—11672.

[30] J. Ma, S. Lindquist, Conversion of PrP to a self-perpetuating PrPSc-like conformation in the cytosol, Science 298 (2002) 1785—1788.

[31] Alessandro Barducci, Riccardo Chelli, Piero Procacci, Vincenzo Schettino, L. Francesco Gervasio, Michele Parrinello, Metadynamics simulation of prion protein: β-structure stability and the early stages of misfolding, J. Am. Chem. Soc. 128 (2006) 2705—2710.

[32] M. Clark, R.D. Cramer, N.V. Opdenbosch, Validation of the general purpose tripos 5.2 force field, J. Comput. Chem. 10 (1989) 982—1012.

[33] J. Gasteiger, M. Marsili, Tetrahedron 36 (1980) 3219—3228.

[34] N.J. Richmond, C.A. Abram, P.R. Wolohan, E. Abrahamian, P. Willett, R.D. Clark, GALAHAD: 1 pharmacophore identification by hypermolecular alignment of ligands in 3D, J. Comput. Aided Mol. Des. 20 (2006) 567—587.

[35] J.K. Sheppird, R.D. Clark, A marriage made in torsional space: using GALAHAD models to drive pharmacophore multiplet searches, J. Comput. Aided Mol. Des. 20 (2006) 763—771.

[36] R.D. Cramer, D.E. Patterson, J.D. Bunce, Comparative molecular field analysis (CoMFA), effect of shape on binding of steroids to carrier proteins, J. Am. Chem. Soc. 110 (1988) 5959—5967.

[37] A. Onufriev, D. Bashford, D.A. Case, Modification of the generalized born model suitable for macromolecules, J. Phys. Chem. B 104 (2000) 3712—3720.

[38] S. Wold, Validation of QSAR's, QSAR 10 (1991) 191—193.

[39] J. Shao, Linear model selection by cross-validation, J. Am. Stat. Assoc. 88 (1993) 486—494.

[40] R.D. Clark, P.C. Fox, Statistical variation in scrambling, J. Comput. Aided Mol. Des. 18 (2004) 563—576.

[41] J.M. Luco, F.H. Ferretti, QSAR based on multiple linear regression and PLS methods for the anti-HIV activity of a large group of HEPT derivatives, J. Chem. Inf. Comput. Sci. 37 (1997) 392—401.

[42] G. Cruciani, M. Baroni, S. Clementi, G. Costantino, D. Riganelli, B. Skagerberg, Predictive ability of regression models. Part I: standard deviation of prediction errors (SDEP), J. Chemom. 6 (1992) 335—346.

[43] M. Baroni, S. Clementi, G. Cruciani, G. Costantino, D. Rainelle, E. Oberrauch, Predictive ability of regression models. Part II: selection of the best predictive PLS model, J. Chemom. 6 (1992) 347—356.

[44] A.D. Mackerell, M. Feig, C.L. Brooks, Extending the treatment of backbone energetics in protein force fields: limitations of gas-phase quantum mechanics in reproducing protein conformational distributions in molecular dynamics simulations, J. Comput. Chem. 25 (2004) 1400—1415.

[45] R.P. Sheridan, M.D. Miller, D.J. Underwood, S.K. Kearsley, Chemical similarity using geometric atom pair descriptors, J. Chem. Inf. Comput. Sci. 36 (1996) 1.

[46] C.A. Gatti, P.H. Risso, M.S. Pires, Spectrofluorometric study on surface hydrophobicity of bovine casein micelles in suspension and during enzymatic coagulation, J. Agric. Food Chem. 43 (1995) 2339—2344.